Surface acoustic wave induced particle manipulation in a PDMS channel—principle concepts for continuous flow applications

**Linda Johansson · Johannes Enlund ·
Stefan Johansson · Ilia Katardjiev · Ventsislav Yantchev**

Abstract A device for acoustic particle manipulation in the 40 MHz range for continuous-flow operation in a 50 μm wide PDMS channel has been evaluated. Unidirectional interdigital transducers on a Y-cut Z-propagation lithium nixobate wafer were used to excite a surface acoustic wave that generated an acoustic standing wave inside the microfluidic channel. It was shown that particle alignment nodes with different inter-node spacing could be obtained, depending on device design and driving frequency. The observed inter-node spacing differed from the standard half-wavelength inter-node spacing generally employed in bulk acoustic transducer excited resonant systems. This effect and the related issue of acoustic node positions relative the channel walls, which is fundamental for most continuous flow particle manipulation operations in channels, was evaluated in measurements and simulations. Specific applications of particle separation and alignment where these systems can offer benefits relative state-of the art designs were identified.

Keywords Acoustic particle manipulation · Ultrasound · PDMS · Surface acoustic wave · Particle alignment

L. Johansson (✉) · J. Enlund · S. Johansson · I. Katardjiev ·
V. Yantchev
Department of Engineering Sciences, Ångström Laboratory,
Uppsala University,
PO Box 534, SE-75121 Uppsala, Sweden
e-mail: johansson.lek@gmail.com

L. Johansson
Department of Applied Physics, Albanova/KTH,
Roslagsv. 30B,
SE-114 19 Stockholm, Sweden

In continuous-flow microfluidic systems, acoustic radiation forces have been exploited in particle manipulation applications such as separation, sorting, trapping and alignment (Petersson et al. 2004; Hawkes and Coakley 2001; Bazou et al. 2008; Johansson et al. 2009; Townsend et al. 2008). Typically, the transducer employed is a bulk acoustic wave (BAW) transducer, positioned as one of the channel walls (Lilliehorn et al. 2005), in contact with a coupling layer close to the acoustic zone (Hawkes and Coakley 2001; Haake and Dual 2005) or at some distance (Nilsson et al. 2004; Wiklund et al. 2006). More recently, surface acoustic wave (SAW) transducers have been used for particle alignment by acoustic radiation forces; in droplets (Li et al. 2008) in larger wall-less chambers (Seemann et al. 2006; Wood et al. 2008, 2009) and alignment in continuous-flow systems. Specifically, particle alignment in continuous-flow systems has been performed in a superstrate poly-di-metyl-siloxane (PDMS) channel at approximately 40 MHz (Shi et al. 2008a) and at 20 MHz (Shi et al. 2008b) and two-particle separation (0.87 μm from 4.17 μm diameter polystyrene particles) (Shi et al. 2009a), at 140 MHz for droplet sorting (Franke et al. 2009) and cell sorting by acoustic streaming (Franke et al. 2010). Additionally, in a superstrate fused silica channel SAW-excited sub-μm particle (0.5 μm diameter polystyrene) alignment has been demonstrated by use of Stoneley wave (Yantchev et al. 2010). In a channel fabricated in the piezoelectric substrate by laser alignment to one side of the channel simultaneous to fluid propulsion by acoustic streaming has been realised by a SAW transducer (Tan et al. 2009). Particles have also been manipulated by SAW-excited acoustic streaming inside droplets (Tan et al. 2007) and indirectly when enclosed in droplets that are manipulated (Franke et al. 2009). In addition, SAW-induced acoustic streaming has been used for fluid manipulation by mixing, droplet

transport, ejection and atomization at increasing voltage levels (Yeo et al. 2009).

The work presented here evaluates coupling mechanisms and nodal patterns in SAW-based particle manipulation in PDMS superstrate channels, which are effects not fully understood or previously studied in detail. Control of the acoustic node positions relative the channel walls is fundamental for most continuous flow particle manipulation operations in channels, such as alignment prior to sensor detection or in combination with a flow split outlet for particle-particle or particle-fluid manipulation for separation, enrichment, fluid washing etc. While SAW-excited particle alignment in PDMS channels has been previously demonstrated by Shi et al. (2008a, b, 2009a, b) and Nam et al. (2011) the significance of the alignment node position relative the channel walls for different types of particles has not been addressed. A related question regards the transport of energy to the fluid layer. SAW-excited particle manipulation in channels, as opposed to in droplets, requires energy transport via a channel structure into the fluid layer. The channel material can influence the energy coupling into the fluid layer as well as providing boundary conditions for the fluidic cavity, thereby affect the appearance of the acoustic field in the fluidic layer. Since PDMS imposes fundamentally different acoustic properties compared with conventional glass or silicon channel BAW transducer systems it is of interest to investigate what is the principle of operation for these systems.
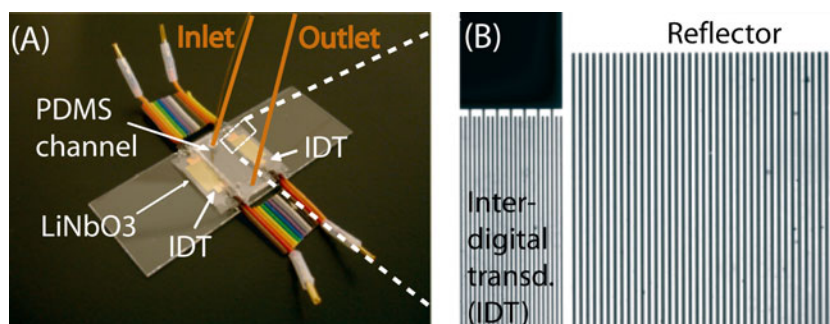
The principle design of the system is shown in Fig. 1. Two interdigital transducers (IDT) are typically used to generate two counter-propagating waves that creates a standing wave inside the microfluidic layer.

Half wavelength width channels with pressure anti-nodes at glass channel walls has been most commonly used in literature for acoustic manipulation (Nilsson et al. 2004; Harris et al. 2003; Hawkes et al. 2004). The particles are moved to one middle node or to two side nodes. The opposite case, with a pressure node at the channel walls has been obtained in a quarter-wavelength channel (Townsend

et al. 2008), but careful layer design and high thickness control is required (Hill 2003). The control of the node positions is especially important if sheath-less operation is desired or if a high degree of enrichment is desired. Operation without sheath flow is important where portability and easy fluidics is emphasized. A high degree of enrichment is desired for instance in rare sample enrichments. Additionally, control of the acoustic node positions is strongly related to factors such as system reproducibility and fabrication alignment tolerances.

Several interesting device and system properties are envisioned for the systems based on lithium niobate (LiNbO$_3$) SAW transducers compared with piezoceramic PbZr$_{(1-x)}$Ti$_x$O$_3$ (PZT) BAW transducers. For SAW devices a larger frequency interval is accessible than for BAW devices. Especially high frequency operation is interesting since the acoustic radiation force scales with frequency for a given acoustic pressure level. The lithium niobate is associated with low material losses and hence does not generate any considerable temperature increase in the actuator material at the employed power levels. The manufacturing process is compatible with planar micro fabrication techniques and the position of the IDTs outside the channel enables a thin transparent device for easy inspection. The large aperture of the IDT relative the wavelength enables a uniform excitation along the channel and little divergence of the acoustic field and therefore potentially a uniform acoustic field in the channel. The power density of a SAW is high, in the range of 100 W/cm^2 (Kurosawa et al. 2003) and the coupling of a SAW from the piezoelectric substrate into the fluid by a leaky wave is an efficient coupling mechanism. Part of the interest for SAW-devices for acoustic manipulation is also related to possibilities for integration realisation in Lab-on-a-chip and Point-of-care-systems.

In this work, a finite element method (FEM) is used to visualise in 2D acoustic fields in a simplified model, which are compared with the observed particle alignment results. Analysis of SAW-excited particle manipulation has also been performed by ray tracing method (Huang et al. 2011).

Fig. 1 (a) System set-up with the gold IDT structure on the lithium niobate substrate and the PDMS channel superstrate mounted on a microscope glass slide. Fluidic inlet was provided by a glass capillary. By connecting the electrical connections on one side the two IDTs were operated in series. (b) Close-up of the top region of one of the sets of IDT strips and the reflector strips

Based on the simulation results, principle routes to controlled and efficient particle manipulation in SAW-excited PDMS channels are presented. It will be demonstrated that for these systems, the acoustic nodes are placed opposite to the traditional case of BAW-transducer glass half wavelength channel systems. Additionally, that the inter-node distances not always corresponds to half the wavelengths in water or in the SAW substrate. The work presented here is a step towards better understanding of particle manipulation in PDMS channels excited by surface acoustic waves. In addition, a novel principle for particle manipulation is demonstrated where the channel and the IDTs are aligned at an angle. The presented system offers increased system power efficiency by unidirectionality of the interdigital transducer (IDT). In this work a flow-split was designed for extracting a small part of the flow at high frequency operation for addressing separation of particles relative other particles and relative fluid in addition to particle alignment.

1 Theory and principles

1.1 The acoustic radiation force

To obtain strong acoustic radiation forces, a standing acoustic field is required inside the fluid. The two IDTs excite SAWs that propagate towards the channel in opposite directions and generate an acoustic field in the fluid layer, Fig. 1. For an arbitrary field, the time-averaged acoustic radiation potential (generally labelled 'primary' or 'direct'), U, arising due to the non-linearity in the propagation of acoustic waves in fluids, that was derived by Gorkov (1962) and may be expressed (Wiklund and Hertz 2006) as

$$\langle U \rangle = \frac{4\pi r^3}{3} \left(f_1 \langle E_{pot} \rangle - f_2 \frac{3}{2} \langle E_{kin} \rangle \right), \tag{1}$$

where the material dependent contrast factors f_1 and f_2 are

$$f_1 = 1 \frac{\rho_0 c_0^2}{\rho c^2}, f_2 = \frac{2(\rho - \rho_0)}{2\rho + \rho_0}, \tag{2}$$

and the time-averaged potential and kinetic densities are

$$\langle E_{pot} \rangle = \frac{\langle p^2 \rangle}{2\rho_0 c_0^2}, \langle E_{kin} \rangle = \frac{\rho_0 \langle v^2 \rangle}{2}, \tag{3}$$

for the pressure amplitude due to the sound, p, and the velocity amplitude due to the sound, v, the density in the absence of sound, ρ, and the sound velocity of the medium, c. The index 0 refers to the medium while no index is used for the particle. Compressible spherical particles are assumed, no acoustic scattering effects from walls are accounted for and the expression is valid under the requirement that particles are small relative the wavelength

(Wiklund and Hertz 2006). Provided that the pressure and velocity amplitudes are known, the radiation force is obtained as the spatial gradient of the acoustic potential at that point. While the radiation force determines the strength of the acoustic manipulation effect, the acoustic potential field, U, where F=−dU/dx, displays the positions at which the particles will be gathered. The particles will move to potential minima and be repelled from regions of positive acoustic potential (Wiklund and Hertz 2006). A particle with positive acoustic contrast factor, θ, $(\theta=f1+3/2f2)$ will move to the pressure node while a particle with negative acoustic contrast factor will move to the pressure anti-node.

1.2 FEM simulations

1.2.1 Acoustic field

Finite Element Model (FEM) simulations (Comsol Multiphysics 4.1) were performed to study the acoustic potential fields in the fluid layer. The device cross-section was modelled in 2D in a frequency analysis. A simplified IDT-electrode geometry of four periods of electrodes stripes were used, with altering potential and ground (+−+ −) positioned on either side of the PDMS structure and excited by a sinusoidal potential of 10 V. The mesh size used was 1 μm in PDMS and water layer, 5 μm in central LiNbO3 layer, corresponding generally to more than 12 mesh elements per wavelength. Because of the high Poisson's ratio of approximately 0.49 in PDMS, the "Mixed U-P formulation" was activated in the program.

PDMS is a hyper elastic and viscoelastic material. For the small signals employed it is straight forward to omit the hyperelastic properties of PDMS. The viscoelastic material properties can in principle be taken into account by using an elastic model in frequency analysis but with complex values of Young's Modulus and Poisson's ratio. The complex modulus have a dynamic real part that increases with frequency until it reaches a plateau and a lossy part that displays a peak (Pritz 1998). Poisson's loss factor is small also for elastomers with high shear damping (Pritz 2007) and is here omitted.

Generally, the Poisson's ratio and Young's modulus can be calculated from measurements of longitudinal and shear velocities. At 5 MHz for RT 601, the longitudinal sound speed is 1030 m/s and the density is 1070 kg/m (Zell et al. 2007). However, publications of shear velocity of PDMS are scarce in the literature because of the high absorption losses of the shear wave. For another PDMS material (Silicone RT 615, Wacker) with somewhat lower static shear modulus than TR 601 (0.8 MPa versus 1.5 MPa) the shear velocity is reported to be in the range of 100 m/s at 10 MHz (Madsen et al. 1983). Using shear velocity of 100 m/s and density of 1080 kg/m (as specified by Wacker) yields Poisson's ratio of 0.495 (υ=(3 K'-2 G')/(2(3 K'+G'),

$c_S^2 = G'/\rho$, $c_L^2 = (K'-4/3\ G')/\rho)$ and Young's Modulus of 30 MPa ($E = 3\ K(1-2\upsilon)$). Note that this dynamic value of Young's Modulus is several times higher than the static value. An error in Poisson's ratio has large impact on the calculation of the absolute value of Young's Modulus.

At increasing frequency for viscoelastic materials, Young's Modulus increases and Poisson's ratio decreases. Regarding the decrease of Poisson's ratio, for most materials it is small enough to be omitted around the frequency interval of interest. According to calculations by Pritz (2007), 1% decrease is for polyurethane rubber found between 10 kHz to 10 MHz (Mott et al. 2002), and for Styrene-Butadiene rubber between 10 MHz to 50 MHz (Wada et al. 1962). Regarding the increase in Young's Modulus with frequency, it is expected that at 40 MHz Young's Modulus will be somewhat higher than at 5 MHz. Several factors such as type of PDMS material, variations in curing agent to mixing ratio, the degree of curing, the curing temperature etc. are also expected to influence the value of Young's Modulus. In the FEM simulations, a Young's Modulus of 5, 10, 20 and 30 MPa for the PDMS was evaluated.

Despite the uncertainty in the PDMS material data, the simulation may still be accurate enough to qualitatively visualise fundamental effects in the acoustic field in the fluid. The low acoustic impedance of PDMS is significant because it ideally generates a pressure-release boundary at the water interface. The acoustic impedance of PDMS (Elastosil RT 601) is in the range of 1.1 MRayl for measurements at 5 MHz (Zell et al. 2007), i.e. lower than for water of 1.5 MRayl. For a material with such low acoustic impedance the high acoustic contrast particles is expected to gather at the PDMS walls in a cavity supporting a plane standing wave.

For simplicity only a few wavelengths of the PDMS solid was modelled since the wave propagating in the PDMS structure will generate a periodic pattern. The inner PDMS layer was selected to approximately 200 μm (1.5 or 2 wavelengths of the SAW) on either side of the fluid layer and approximately 150 μm in the height direction. Material losses of the PDMS material (Elastosil RT 601) in the range 4–14 MHz display a high attenuation coefficient for the longitudinal wave, $\alpha = 6.06f^{0.49}$ (Zell et al. 2007). Assuming this relation is valid also at 40 MHz, longitudinal losses are in the range of 400 m^{-1} and the pressure amplitude decreases by approximately 50% in 1.5 mm. Hence, the acoustic field in the fluid is expected to be influenced by the surrounding PDMS region of about 1.5 mm. It is expected that acoustic energy mainly reaches the fluid directly from the substrate or after propagating a shorter distance in the PDMS. However, per wavelength the decrease in pressure amplitude is only 5%. In the inner PDMS layer a lower loss factor of 0.1 was used. In the height direction the PDMS layer is approximately 4 mm thick and after 8 mm propagation in a roundtrip

approximately 20% of the energy ideally can return to the PDMS-fluid interface.

The outer parts of the PDMS solid were modelled as an absorbing region, with an isotropic loss factor of 0.9. At the boundary between the two PDMS layer part of the wave is reflected, as opposed to a well designed perfectly matched layer (PML). Hence a degree of reflection is included in the model. The outer PDMS-layer was surrounded by an air layer.

Two geometric cases for channel position were considered, *Design A* and *Design B*, and compared with measurements for the two devices presented, *Case i* and *Case ii*. In *Design A*, the fluidic layer was positioned symmetric relative the IDTs and the PDMS channel. In *Design B*, the fluidic layer was shifted 25 μm towards one of the IDTs, corresponding to approximately a quarter wavelength offset relative the SAW in the piezoelectric layer. *Design A* and *Design B* give opposite boundary conditions on the lower boundary of the fluidic cavity. The relatively small change in the manual alignment of the PDMS channel of 25 μm causes the difference between *Design A* and *Design B*. Other alignment cases exist as well, but the selected cases are ideal cases in terms of the fluid layer relative the IDTs and PDMS layer.

1.2.2 Trifurcation outlet design for high enrichment

A flow-split was designed for extracting a small part of the flow at high frequency operation for addressing particle-fluid separation in addition to particle alignment. The modified trifurcation flow-split outlet design was simulated in FEM (Comsol Multiphysics 3.4) to illustrate the efficient separation. Equal pressure was assumed at the three channel outlets.

2 Experimental arrangements

2.1 Device design

Several aspects were considered before selecting the operation frequency of approximately 40 MHz. A common concern is the viscous absorption, which increases with frequency. In a water layer of 100 μm at 10 MHz it is less than 0.1% and though several times larger at 40 MHz it is still less than 1% (Kinsler 2000). Regarding the lower frequency limit for a SAW device, the thickness of the piezoelectric substrate will generally need to be at least a few wavelengths for the surface wave to exits (requiring ideally no influence of the substrate edges). Besides channel size and substrate thickness, the selection of operation frequency will also be determined by the minimal IDT electrode width in the lithography step. Additionally, a high frequency IDT has a smaller footprint which also reduces the material cost of the device.
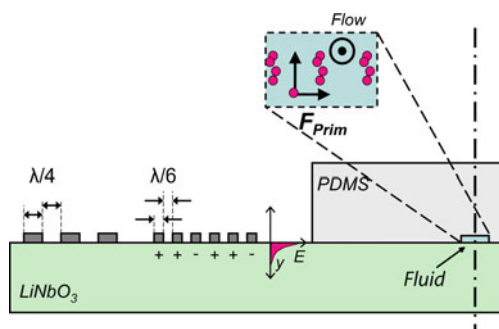
As opposed to isotropically etched channels, PDMS allows easy structuring of channel outlet designs. Hence, pressure driven flow can be used in combination with varying channel widths to ensure for instance high enrichment rate. This is useful for applications where otherwise repeated separation operations or very well-controlled push and pull fluidics are necessary to obtain the desired enrichment rate.

The principal set-up of the interdigital transducer (IDT) on the lithium niobate (LiNbO$_3$) substrate is shown in Fig. 2. 120 IDT electrode strips are organized into 40 pairs with period of one wavelength and potential (++ −). The frequency of operation is determined by the sound velocity divided by the wavelength that is defined by the electrode period of 96 μm. The spacing and width of the electrodes are 1/6 wavelength, i.e. 16 μm. For this case, the electrodes are non-reflecting and therefore no energy is trapped underneath the electrode structure. A reflector structure of 40 stripes with quarter wavelength spacing is positioned on the outer side of each transducer to enable a certain degree of unidirectionality. The waves interfere constructively upon reflection at the electrode edges. By a relatively low number of electrode stripes, the IDT is designed to be a broadband transducer with a Q-value in the range of 20.

The two IDT's with their respective reflectors have an aperture of 9 mm and are placed symmetrically at a distance of approximately 5 mm from the channel on the piezoelectric substrate. The PDMS channel is positioned manually with an estimated accuracy <1 mm.

2.2 Device fabrication

The interdigital transducer (IDT) was fabricated on a 100 mm Y-cut Z-propagating LiNbO$_3$ wafer by e-beam lift-off lithography. Prior to metal deposition, the wafer was cleaned in 1:1 H$_2$SO$_4$:H$_2$O$_2$ piranha wash to remove any residual

Fig. 2 Cross-section of the device showing the reflector strips (λ/4), the IDT strips (λ/6) (with applied electric potential) on the piezoelectric substrate and the PDMS channel in which the acoustic radiation forces causes alignment of the particles in the fluid cavity. The energy distribution, E, of the surface acoustic wave (SAW) as it propagates towards the channel structure is indicated as well as the fluid flow direction and the directions of the primary radiation force, $F_{Prim,}$ in the cross-section plane

surface contaminants. To enhance adhesion of the Shipley 1813 positive photoresist, a primer treatment was performed prior to resist application. After pattern replication, the wafer was cleaned in low-power oxygen/nitrogen plasma to remove residual resist and promote metal adhesion. The Au/Ti (80 nm/10 nm) IDTs was deposited by e-beam evaporation at a base pressure of 2e–6 mBar. To remove the photoresist and finalize the IDT metal pattern, the wafer was immersed in an ultrasonic acetone bath. In a similar manner, Cu/Ti (200 nm/10 nm) contact pads were defined using e-beam lithography.

The channel structure was manufactured by soft lithography of PDMS (Elastosil RT 601, Wacker). The channel width and height were 50 μm and the channel length approximately 1 cm, which was slightly longer than the IDT aperture of 9 mm. The thickness of the PDMS layer was approximately 4 mm. The PDMS base and curing agents were mixed (1:10 v/vt) and degassed in a freezer for a few hours. The PDMS was cast in a SU-8 mould and cured (70°C, 2 h) subsequent to making the fluidic inlets and separating into individual devices by knife with a width of approximately 0.9 cm. The PDMS surface was oxidized by corona discharge while the lithium niobate was oxidized by ashing (150 W, 5 min), in order not to destroy the electrodes. The channel structures were manually aligned and heat treated to strengthen the initial bond (70°C, 48 h) which also significantly reduces the amount of un-cured monomers (Huikko et al. 2003) that otherwise is the main origin of recovery of the hydrophobicity of the oxidized PDMS surface (Kim et al. 2000).

Fluidic connection was provided by gluing a short polyethylene tubing of 380 μm inner diameter (Intramedic BD, Becton Dickinson) outside a glass capillary (outer diameter 365 μm and inner diameter 95 μm). Electrical connections were provided by conductive epoxy (Circuitworks, Chemtronics) covered by epoxy (Plastic Padding) for mechanical robustness. By connecting the electrodes on one side of the device, the transducers were operated in series at half the input voltage each. The device was glued onto a glass slide for fitting into the microscope holder.

2.3 Set-up and quantification

The transducers were excited by a high-frequency function generator (Hewlett-Packard 8116A Pulse/Function generator) with maximum power output of 320 mW or 16 Vpp for a 50Ω load. The minimal step size of this device was 0.1 MHz An Agilent 4395A Network Analyzer was used for impedance measurements (0.22 V at 50 Ω). The ability to manipulate particles was evaluated by observing the particle alignment by an inverted Nikon TE-2000-U fluorescence microscope (Hg-lamp excitation) with a high sensitive cooled CCD camera (Spot Diagnostic Instruments). Initially the channels where filled with ethanol since the applied pressure required for filling the channels

is lower than for water. A syringe pump (Univentor 864) was used with a 100 mL Hamilton syringe.

Three particles were evaluated: negative-θ fat particles (milk, 0.5% fat, Arla Foods AB) and positive-θ green fluorescing 1.9 μm and 0.5 μm polystyrene beads (Polymer Microspheres, Duke Scientific Corp.) of 1.05 g/cm³ density in de-ionized water with 0.5% (v/v) Tween (to prevent particle agglomeration). The flow velocities evaluated were 0.03–0.05 μL/min (12–20 mm/s).
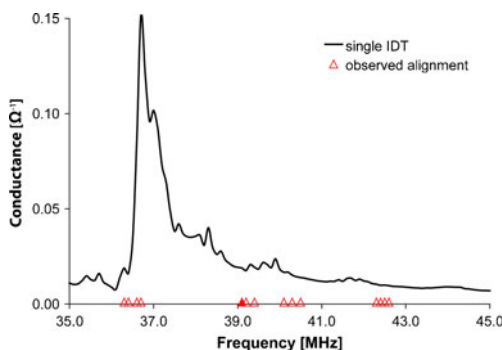
Results from two devices are presented, differing slightly in terms of PDMS channel width and alignment position due to the manual fabrication steps of channel separation and alignment.

3 Results and discussion

The conductance spectra of a single IDT is shown in Fig. 3. The main resonance peak of the IDTs is found at 36.7 MHz. The 40 pairs (l20 strips) of electrodes yield a transducer bandwidth in the range of 1 MHz as is also observed in the graph. The conductance spectrum for the second device was equivalent.

The fastest particle alignment into clear nodes for the two devices was found at 39.1,'Case i', and 38.9 MHz,,'Case ii', respectively (indicated by a filled triangle in Fig. 3 for the 39.1 MHz-device). Other frequencies in the range 35–45 MHz also enabled alignment of all particles before the particles had reached the end of the channel, however less fast, (indicated by triangles in Fig. 3). The frequencies with observed particle alignment have conductance close to the 0.02 Ω⁻¹ which enables good coupling from the generator. Factors affecting the wave path length from the two IDTs will influence which frequencies yield particle alignment. For instance, the position of the channel relative the IDT and the PDMS side-wall thickness influence the degree of the constructive interference at a certain frequency.

For device operated at 38.9 MHz-channel, *Case i*, the negative-θ particles were observed to align to two anti-node

Fig. 3 The conductance versus frequency spectrum for the 39.1 MHz-device in single IDT operation. Alignment was observed at several frequencies (*triangles*) and was best at 39.1 MHz (*filled triangle*)
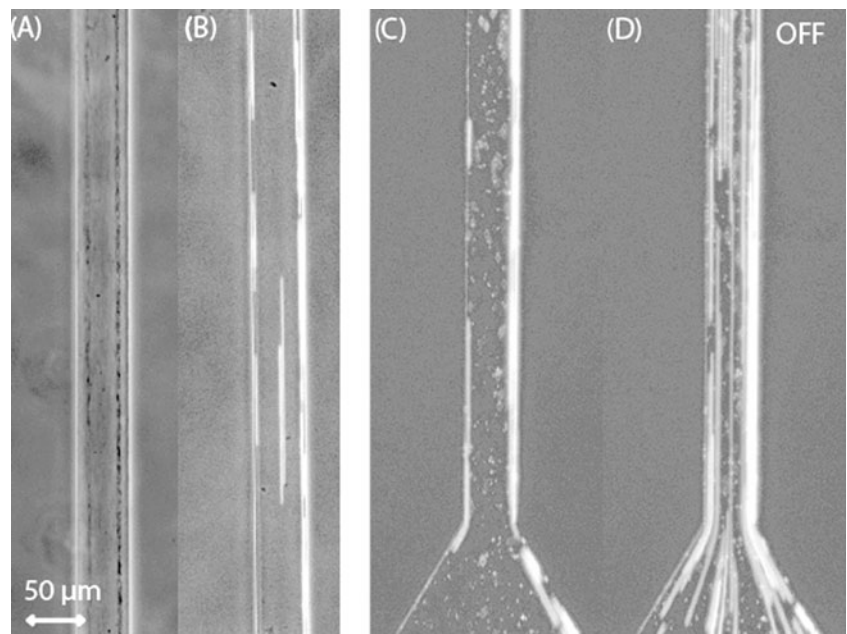
positions a certain distance from the channel walls, Fig. 4(a), i.e. an inter-node distance somewhat less than a half wavelength of the SAW. For the positive-θ particles, the alignment was observed to occur to three nodes: at the channel walls and the channel middle, Fig. 4(b), i.e. possibly an inter-node distance significantly less than a half wavelength of the SAW. The flow rate was *0.03 μL/min (12 mm/s)*. It was not observed weather the alignment also occurred in the vertical direction. For the smaller polystyrene particles of 0.5 μm diameter, which are subject to lower acoustic radiation forces, no alignment was observed.

For the device operated at 39.1 MHz-channel, case *ii*, the alignment of positive-θ particles was observed to occur to two nodes, at the channel edges, Fig. 4(c), as opposed to OFF in Fig. 4(d). The flow rate was 0.05 μL/min (20 mm/s). This corresponds to an internode distance of 50 μm, or larger. Half-wavelength internode distance is similar to IDT-excitation into a PDMS-channel presented elsewhere (Shi et al. 2008b) and a cavity without side-walls (Wood et al. 2008).

The FEM-simulation of *Design A* (symmetric) and *Design B* (offset) for Young's modulus of 10 MPa are shown in Fig. 5. The displacement amplitude displays a periodic pattern of a standing wave in the lithium niobate. The amplitude of the displacement is observed to change for different plot angles so it is not a perfect standing wave. A displacement maximum in the substrate generated a pressure amplitude maxima in a standing acoustic field at the PDMS interface. The pressure amplitude in the PDMS extends some distance into the PDMS before it decrease, depending on the loss factor. The fluid layer disturbs the acoustic field in the PDMS interface region. At the fluid layer the vertically oriented pattern in the PDMS changes to an angular orientation directed from the fluid layer. A weak standing wave is found in the PDMS as a result of reflections at the upper PDMS absorption layer, Fig. 5(a) and (b). Displacement maxima are found at the upper boundary interfacing the absorbing PDMS region. It is a pressure-release boundary, as would also be found at an air interface. The height of the inner PDMS layer encompasses several multiples of λ/2. In the high loss PDMS region the amplitude is damped within a short distance. The simulation frequencies in Fig. 5(a) and (b) are close to the measurement frequencies, but not exactly the same. The frequencies selected most clearly display the observed measurement pattern. One origin of the frequency discrepancy is deviations in geometry between the device and the simulation model. In general, a similar appearance of the acoustic pattern is found in a frequency interval.
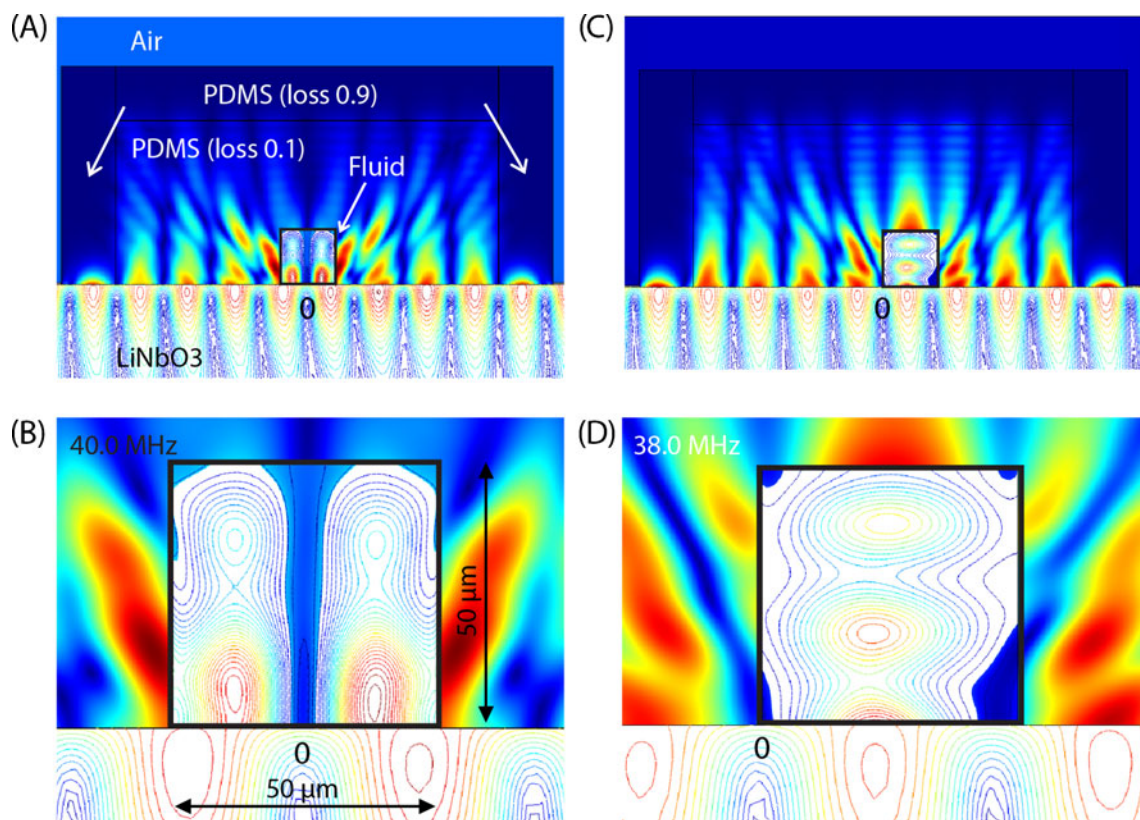
For *Design A*, the position of the fluid side walls coincides with a displacement maxima in the piezoelectric layer. The generated acoustic potential in the fluid layer displays minima in a narrow line in the middle of the

Fig. 4 Photo of the alignment of fat particles (*dark*) and 1.9 μm fluorescent polystyrene beads (*white*) relative the channel walls in the 50 μm wide channels for the Case i (38.9 MHz), (**a** and **b**), and the Case ii (39.1 MHz) (**c** and **d**). For the case i, (**a**) fat particles (negative acoustic contrast factor) aligned into two lines positioned some distance from the walls and (**b**) 1.9 μm polystyrene beads (positive acoustic contrast factor) aligned into three lines positioned at the walls and the channel-middle, for a flow rate of 0.03 μL/min (12 mm/s). For the case ii, (**c**) 1.9 μm polystyrene beads aligned into two nodes (**d**) as opposed to when the transducer was OFF, for a flow rate of 0.05 μL/min (20 mm/s)

channel and at regions at the channel side walls, Fig. 5(c), in agreement with the measurements. The positions of the

acoustic potential maxima, which indicate where particles with opposite acoustic contrast factor would go, are in

Fig. 5 FEM-simulation results for (**a**) "Design A" at 40.0 MHz and (**c**) "Design B" at 38.0 MHz of displacement amplitude in the piezoelectric material, pressure amplitude in the PDMS layers and acoustic potential in the fluid for the 1.9 μm polystyrene particles (red colour=maximum value, blue colour=minimum value). Close-up (**b**) "Design A"and (**d**) "Design B" of the fluid layer with lower potential regions filled. The absolute values are low since only few IDT strips are modelled. Maximum displacement amplitude is in the range of 0.3 nm, maximum pressure amplitude in the range of 0.1 MPa and acoustic potential in the range of −0.1–1 aN (Design A) and −0.3–3 aN (Design B)

agreement with the observed alignment positions for the fat particles. At the centre position a displacement minima is found in the substrate and an acoustic potential minima for polystyrene particles in the fluid layer, i.e. a pressure node. In vertical direction, the lower maxima and minima are both found some distance above the bottom fluid wall. This was not possible to verify in the experiment but is an advantageous characteristic since particles travelling away from the walls are less susceptible to sticking.

For higher isotropic losses in the inner PDMS layer of 0.5 no reflections are found at the PDMS-PDMS boundary and no vertical standing wave is obtained in the inner PDMS layer. However, the appearance of the acoustic field inside the fluid qualitatively remains the same for both *Design A* and *Design B*.

For *Design B*, the position of the fluid side walls coincides with a displacement maxima in the piezoelectric layer. The generated acoustic potential in the fluid layer displays potential minimum at two regions close to the fluid side walls, Fig. 5(d), in agreement with the experiment. At the centre position a displacement maxima is found in the substrate and an acoustic potential maxima for polystyrene particles in the fluid layer, i.e. a pressure anti-node. The geometry in *Design B* generate a slightly non-symmetric acoustic field in the fluid for this design at this frequency.

The simulation examples in *Design A* and *Design B* gives a possible explanation to the initially puzzling observation of different internode spacing for the two devices presented. It is expected that the node position relative the channel walls will differ between devices, since the acoustic path length depend on the exact position of the PDMS channel which is not very accurately controlled for the manual alignment method employed. It is observed from simulations that by altering the phase of one of the IDTs, the position of the nodes in the SSAW are shifted. By adding 180 deg phase lag to one IDT, the pattern in Fig. 5(c) is observed for the *Design B* case and the pattern in Fig. 5(d) is observed for *Design A*. Hence, a phase shift at one of the IDTs can be used to align the acoustic field relative the position of the fluidic channel. This is a great advantage reducing the requirements of alignment during manufacturing but was not possible to verify in the measurements.

For lower values of Young's Modulus, 5 MPa, the same principle appearance of the acoustic field is obtained. At 20 MPa and 30 MPa, *Design A* does not generate results corresponding to the measurements.

When the SAW encounters a PDMS/LiNbO$_3$-interface, part of the energy radiates into the PDMS layer at an angle while part of the energy propagates along the substrate surface. As the wave propagates, more and more of the energy will couple into the PDMS bulk. If the material losses are not too high, acoustic modes in the PDMS bulk may be excited. The counter-propagating waves in the substrate generates a standing wave. A standing acoustic field is generated in the PDMS layer with pressure amplitude maxima at the displacement maxima in the substrate. At the fluid interface, a pressure field inside the fluid is excited at the bottom substrate and also at the cavity side-walls. The energy coupled into the fluid layer is also believed to radiate out into the PDMS layer. The acoustic potential in the fluid is generated by the standing wave, as an interference pattern from counter-propagating waves. The boundary conditions of the fluidic cavity have an impact on the appearance of the acoustic field in the fluid.

The particles were observed to align to a narrow focus region estimated to 14% of the channel width, i.e. 7 μm. Hence, the voltage levels and channel lengths employed are clearly adequate to accomplish the desired alignment effect at these flow rates. The particles sizes employed here is in the range of the smallest particle sizes usually employed in BAW-transducer systems (usually polystyrene particles larger than 1 μm diameter). It may be expected that a system design optimum exists corresponding to a certain channel width, channel position and channel geometry. However, for these non-optimized devices it is shown that the created acoustic field is strong enough to enable manipulation with different positions of pressure nodes relative the channel walls, depending on the alignment of the channel and the operation frequency and phase.
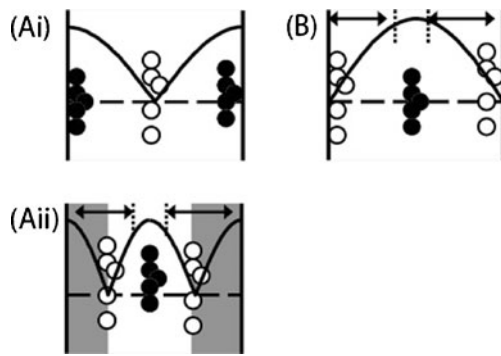
3.1 Identification of application examples

Based on the general principles of operation obtained from the measurements and modelling above for the SAW excited PDMS channel system a description of how to explore these properties in some specific examples of particle separation and alignment are provided to illustrate the significance of the described system properties. For the selected examples, the described system can offer benefits relative state-of the art designs.

3.1.1 Negative acoustic-contrast-factor particles aligned away from the channel walls

In Fig. 6(a(*i*)), the pressure amplitude distribution (solid line) in a typical half-wavelength standing-wave device (Nilsson et al. 2004) is shown in the schematic. The alignment of negative-θ particles (dark) occurs at the channel walls with risk of sticking. One solution is to operate at the 2 λ/2-frequency and introduce a sheath flow, Fig. 6(a(*ii*)). The negative-θ particles can then be aligned to the middle of the channel and hence be separated in a trifurcation outlet without risk of clogging the channel. However, in fluid purification applications the introduction of a sheath flow can be disadvantageous since it dilutes the remaining sample, requires more complex fluidics and a bulky system. One such

Fig. 6 Illustration of different cases of particle alignment in a channel used with trifurcation outlet. The pressure amplitude distribution is indicated by a solid line for (**a**(*i*)) an anti-pressure node at the channel wall and (**b**) a pressure node at the channel wall. (**a**(*i*)) Negative-θ particles (*dark*) align to the channel walls with risk of sticking. (**b**) The same particles align to the channel middle and can be separated without risk of clogging. (**a**(*ii*)) For the channel in (**a**(*i*)) a 2/2λ-frequency can be used in combination with a sheath flow (*grey*) to prevent the particles from contact with the channel walls. However, the introduction of a sheath flow can be disadvantageous since it dilutes the remaining sample, which is avoided in (**b**)

Fig. 7 A modified trifurcation outlet design for extraction of a small part of the middle flow. FEM-simulation with particle traces (*white lines*) for no-slip boundary condition at the channel walls and equal pressure at the channel outlets
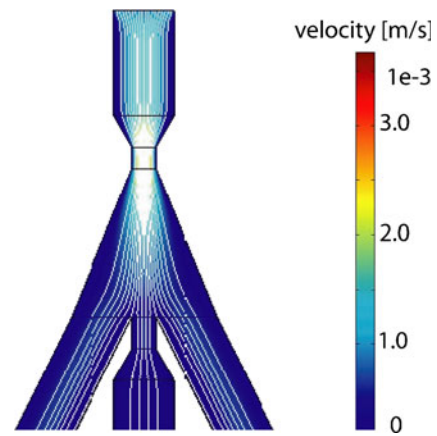
application is the removal of fat particles in milk samples before performing bacterial analysis (Grenvall et al. 2008). Pressure nodes at the channel side-walls are then advantageous and can be achieved by the presented device, Fig. 6(b).

Additionally, for a sample where contact with the channel wall is not an issue, the removal of positive acoustic-contrast-factor particles is more efficient by two side-outlets instead of one middle outlet. Efficient removal of a high concentration of blood cells in plasma-purification may be one such application (Lenshof 2011).

Another case when the device offers benefit is for moving weak negative-acoustic contrast particles into a new fluid. In case of parabolic flow profile, an initial position at the channel side-wall is be beneficial because of slower flow velocity and hence longer residence time for interaction with the acoustic field.

3.1.2 Trifurcation outlet design for high enrichment

The alignment in the evaluated devices occurs into a narrow region, with a width of approximately 7 μm as estimated from Fig. 4. Hence, an outlet design with narrow channels is expected to yield a high enrichment rate. Modelling results of the proposed trifurcation design is shown in Fig. 7. After the narrow acoustic alignment zone, a magnification zone is used to increase the spacing between the fluid streams. In the subsequent step, the narrow middle outlet channel enables separation of a small fluid stream. The subsequent widening of the narrow channel limits the increase in fluidic resistance. The simulation shows that the outlet design enables separation of a small part of the initial volume since only four of the 20 initially equidistant particle traces exit through

the middle outlet. Additionally the channel only presents a short section of larger pressure resistance.

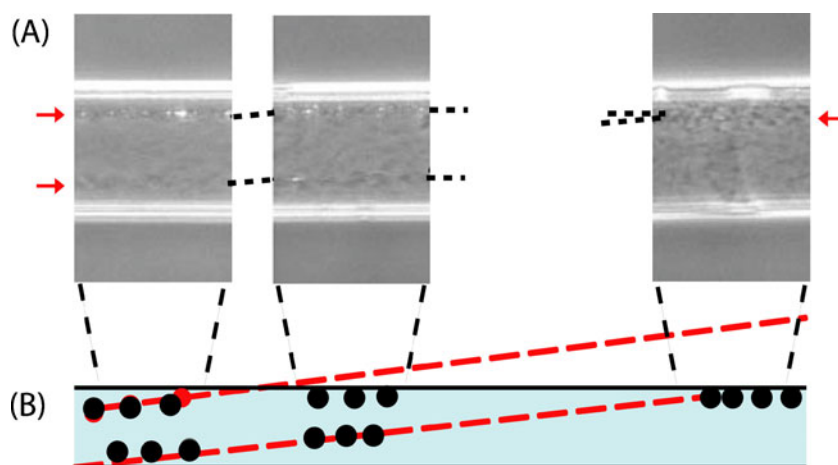### 3.1.3 Aligning all particles to one of the channel walls

When considering the whole channel length, angular off-alignment of the nodes relative the channel walls was observed for the 38.9 MHz-device, but not for the 39.1 MHz-device. In the former case, the nodes were shifted slightly along the channel and at the outlet all particles were positioned at one of the channel walls, as shown for fat particles in Fig. 8(a). The channel angular off-alignment relative the IDTs can be used for positioning particles close to one of the channel walls, as illustrated in the schematic, Fig. 8(b). However, the FEM-model used here is not adequate to fully describe the observed node shift along the channel and the observed angular off-alignment effect. Positioning of coated-beads or spores to sensor surface is one application of interest (Martin et al. 2005). It is envisaged that a sweeping phase at one of the IDTs will shift the particles faster to the sidewall.

3.2 General considerations

The above results show how the issue of channel alignment can be specifically addressed in order to employ the presented system in a predictable manner, both for the case of particle separation and particle alignment to one wall.

Narrow fluidic channels accentuate the effect of surface charges of the channel wall relative the particles or cells and imposes high requirement on the purity of the fluid to avoid clogging. A common scenario during the measurements was that at some point, sometimes after hours of operation, the particles started to agglomerate at a distinctive and short part of the channel wall. Once a few particles were gathered, it was

Fig. 8 (a) Alignment of fat particles along the channel for the 38.9 MHz-device where the channel was slightly off-aligned relative the IDTs. The off-alignment generated a shift of the particle position (indicated by a *black dotted line*) throughout the channel. At the outlet, the fat particles (*black*) which upstream were aligned in two nodes were all positioned at one of the channel walls (flow rate of 0.03 μL/min, 12 mm/s). (b) Illustration of employing channel off-alignment for positioning particles at one of the channel walls

impossible to remove the particles by the flow. Hence, if to be operated for longer times, a PDMS surface treatment is needed. Alternatively, wider channels and lower frequencies can be an option. A 1000 μm thick lithium niobate wafer of would enable operation frequency of 15 MHz.

No degrading effect of the electrodes such as electrode migration etc. was observed, and the device could be operated for hours at 16 Vpp. The voltage across the electrodes measured by an oscilloscope was 8.8 Vpp.

Several studies have shown no detrimental effects on cell viability for acoustic manipulation at the amplitude levels required to perform acoustic manipulation at 1–10 MHz frequency (Ryll et al. 2000; Bazou et al. 2005; Hultstrom et al. 2007; Evander et al. 2007). At 20 MHz frequency and power levels generating acoustic streaming by SAW transducers, yeast cells evaluated in SEM showed no changes in cell shape or size and proliferated well in the following 14 days of cell culturing (Bok et al. 2009). For the same frequency, Osteoblast cells subject to 10 s of acoustic irradiation displayed no loss of viability.

While these studies are performed at 1–20 MHz frequency, the authors do not expect any significant deviation from that result at 40 MHz though it is envisaged that studies of cell viability is needed to confirm this expectation. Temperature increase and mechanical stress caused by oscillation in phase with the acoustic field are factors to be considered regarding cell viability. The temperature increase originating from the piezoelectric material is low for the piezoelectric materials employed here. The acoustic oscillation amplitude required to generate a certain acoustic radiation force is lower at higher operation frequencies according to theory. Whether a higher oscillation frequency affects the cell viability differently or not needs to be evaluated in future studies. For cells much larger than the nodal region there will be an acoustic radiation force also when the particles are aligned to a pressure node.

In general, efficient acoustic design of the total system is required and the value of parameters such as power level, fluid flow rate and channel length need to be selected for the specific application.

4 Conclusions

A device for acoustic manipulation in continuous flow at around 40 MHz frequency in a 50 μm wide PDMS channel was demonstrated. Two unidirectional interdigital transducers on Y-cut Z-propagating lithium niobate were used to excite the wave. The results show, for the first time, that a PDMS channel bonded on a surface acoustic wave substrate, as opposed to a glass channel device, generally align positive acoustic-contrast-factor particles close to the side walls and negative acoustic-contrast-factor particles away from the channel side walls. The presented FEM model proved to be a valuable tool for illustrating possible qualitative appearances of the acoustic field generated by a SAW in a low-acoustic impedance channel material, including the observed internode distances and node positions relative the channel wall. It was shown how to ease the requirements of channel alignment by adding a phase to one of the IDT signals. A new operation principle was demonstrated where channel angular off-alignment enabled gathering of all particles at one of the channel side walls.

References

D. Bazou, G.A. Foster, J.R. Ralphs, W.T. Coakley, Mol. Membr. Biol. **22**, 229–240 (2005)

D. Bazou, E.J. Blain, W.T. Coakley, Mol. Membr. Biol. **25**, 102–U116 (2008)

M. Bok, H.Y. Li, L.Y. Yeo, J.R. Friend, Biotechnol. Bioeng. **103**, 387–401 (2009)

M. Evander, L. Johansson, T. Lilliehorn, J. Piskur, M. Lindvall, S. Johansson, M. Almqvist, T. Laurell, J. Nilsson, Anal. Chem. **79**, 2984–2991 (2007)

T. Franke, A.R. Abate, D.A. Weitz, A. Wixforth, Lab Chip **9**, 2625–2627 (2009)

T. Franke, S. Braunmuller, L. Schmid, A. Wixforth, D.A. Weitz, Lab Chip **10**, 789–794 (2010)

L.P. Gor'kov, Sovjet Physics **6**, 773–775 (1962)

C. Grenvall, P. Augustsson, H. Matsuoka, T. Laurell, μTAS 2008 Conference, Tokyo, 2008

A. Haake, J. Dual, J. Acoust. Soc. Am. **117**, 2752–2760 (2005)

N.R. Harris, M. Hill, S. Beeby, Y. Shen, N.M. White, J.J. Hawkes, W.T. Coakley, Sensor Actuat B-Chem **95**, 425–434 (2003)

J.J. Hawkes, W.T. Coakley, Sensor Actuat B-Chem **75**, 213–222 (2001)

J.J. Hawkes, R.W. Barber, D.R. Emerson, W.T. Coakley, Lab Chip **4**, 446–452 (2004)

M. Hill, J. Acoust. Soc. Am. **114**, 2654–2661 (2003)

T.J. Huang, J.J. Shi, S. Yazdi, S.C.S. Lin, X.Y. Ding, I.K. Chiang, K. Sharp, Lab Chip **11**, 2319–2324 (2011)

K. Huikko, P. Ostman, K. Grigoras, S. Tuomikoski, V.M. Tiainen, A. Soininen, K. Puolanne, A. Manz, S. Franssila, R. Kostiainen, T. Kotiaho, Lab Chip **3**, 67–72 (2003)

J. Hultstrom, O. Manneberg, K. Dopf, H.M. Hertz, H. Brismar, M. Wiklund, Ultrasound Med. Biol. **33**, 145–151 (2007)

L. Johansson, F. Nikolajeff, S. Johansson, S. Thorslund, Anal. Chem. **81**, 5188–5196 (2009)

J. Kim, M.K. Chaudhury, M.J. Owen, J. Colloid Interface Sci. **226**, 231–236 (2000)

L.E. Kinsler, *Fundamentals of acoustics*, 4th edn. (Wiley, New York, 2000)

M.K. Kurosawa, H. Itoh, K. Asai, Ultrasonics **41**, 271–275 (2003)

A. Lenshof, A. Ahmad-Tajudin, K. Järås, A.-M. Swärd-Nilsson, L. Åberg, G. Marko-Varga, J. Malm, H. Lilja, T. Laurell, Anal. Chem. **81**, 6030–3037 (2011)

H.Y. Li, J.R. Friend, L.Y.L. Yeo, Phys. Rev. Lett., **101** (2008)

T. Lilliehorn, U. Simu, M. Nilsson, M. Almqvist, T. Stepinski, T. Laurell, J. Nilsson, S. Johansson, Ultrasonics **43**, 293–303 (2005)

E.L. Madsen, H.J. Sathoff, J.A. Zagzebski, J. Acoust. Soc. Am. **74**, 1346–1355 (1983)

S.P. Martin, R.J. Townsend, L.A. Kuznetsova, K.A.J. Borthwick, M. Hill, M.B. McDonnell, W.T. Coakley, Biosens. Bioelectron. **21**, 758–767 (2005)

P.H. Mott, C.M. Roland, R.D. Corsaro, J. Acoust. Soc. Am. **111**, 1782–1790 (2002)

J. Nam, Y. Lee, S. Shin, Microfluid Nanofluid **11**, 317–326 (2011)

A. Nilsson, F. Petersson, H. Jonsson, T. Laurell, Lab Chip **4**, 131–135 (2004)

F. Petersson, A. Nilsson, C. Holm, H. Jonsson, T. Laurell, Analyst **129**, 938–943 (2004)

T. Pritz, J. Sound Vib. **214**, 83–104 (1998)

T. Pritz, J. Sound Vib. **306**, 790–802 (2007)

T. Ryll, G. Dutina, A. Reyes, J. Gunson, L. Krummen, T. Etcheverry, Biotechnol. Bioeng. **69**, 440–449 (2000)

K.M. Seemann, J. Ebbecke, A. Wixforth, Nanotechnology **17**, 4529–4532 (2006)

J.J. Shi, X.L. Mao, D. Ahmed, A. Colletti, T.J. Huang, Lab Chip **8**, 221–223 (2008a)

J.J. Shi, D. Ahmed, X. Mao, T.J. Huang, Micro Electro Mechanical Systems, 2008. MEMS 2008. IEEE 21st International Conference on, (2008b)

J. Shi, H. Huang, Z. Stratton, Y. Huang, T.J. Huang, Lab Chip **9**, 3354–3359 (2009a)

J. Shi, Y.B. Zheng, T.J. Huang, Micro Electro Mechanical Systems 2009. MEMS 2009. IEEE 22nd International Conference on (2009b)

M.K. Tan, J.R. Friend, L.Y. Yeo, Lab Chip **7**, 618–625 (2007)

M.K. Tan, R. Tjeung, H. Ervin, L.Y. Yeo, J. Friend, Appl. Phys. Lett., **95** (2009)

R.J. Townsend, M. Hill, N.R. Harris, M.B. McDonnell, Ultrasonics **48**, 515–520 (2008)

Y. Wada, H. Ochiai, R. Ito, J Phys Soc Jpn **17**, 213 (1962)

M. Wiklund, H.M. Hertz, Lab Chip **6**, 1279–1292 (2006)

M. Wiklund, C. Gunther, R. Lemor, M. Jager, G. Fuhr, H.M. Hertz, Lab Chip **6**, 1537–1544 (2006)

C.D. Wood, S.D. Evans, J.E. Cunningham, R. O'Rorke, C. Walti, A.G. Davies, Appl. Phys. Lett. **92**, 044104 (2008)

C.D. Wood, J.E. Cunningham, R. O'Rorke, C. Walti, E.H. Linfield, A.G. Davies, S.D. Evans, Appl. Phys. Lett. **94**, 054101 (2009)

V. Yantchev, J. Enlund, I. Katardjiev, L. Johansson, J. Micromech. Microeng., **20** (2010)

L.Y. Yeo, J.R. Friend, Biomicrofluidics, **3** (2009)

K. Zell, J.I. Sperl, M.W. Vogel, R. Niessner, C. Haisch, Phys. Med. Biol. **52**, N475–N484 (2007)